



Piezoelectric control of needle-free transdermal drug delivery

Jeanne C. Stachowiak^a, Marcio G. von Muhlen^b, Thomas H. Li^a,
Laleh Jalilian^b, Sapun H. Parekh^b, Daniel A. Fletcher^{b,c,*}

^a University of California, Berkeley, Department of Mechanical Engineering, Berkeley CA 94720, United States

^b University of California, Berkeley, Department of Bioengineering, Berkeley CA 94720, United States

^c University of California, Berkeley, Biophysics Graduate Group, Berkeley CA 94720, United States

Received 23 June 2007; accepted 16 August 2007

Available online 23 August 2007

Abstract

Transdermal drug delivery occurs primarily through hypodermic needle injections, which cause pain, require a trained administrator, and may contribute to the spread of disease. With the growing number of pharmaceutical therapies requiring transdermal delivery, an effective, safe, and simple needle-free alternative is needed. We present and characterize a needle-free jet injector that employs a piezoelectric actuator to accelerate a micron-scale stream of fluid (40–130 μm diameter) to velocities sufficient for skin penetration and drug delivery (50–160 m/s). Existing jet injectors, powered by compressed springs and gases, are not widely used due to painful injections and poor reliability in skin penetration depth and dose. In contrast, our device offers electronic control of the actuator expansion rate, resulting in direct control of jet velocity and thus the potential for more precise injections. We apply a simple fluid-dynamic model to predict the device response to actuator expansion. Further, we demonstrate that injection parameters including expelled volume, jet pressure, and penetration depth in soft materials vary with actuator expansion rate, but are highly coupled. Finally, we discuss how electronically-controlled jet injectors may enable the decoupling of injection parameters such as penetration depth and dose, improving the reliability of needle-free transdermal drug delivery.

© 2007 Elsevier B.V. All rights reserved.

Keywords: Needle-free injector; Drug delivery; Transdermal; Piezoelectric; Jet injector

1. Introduction

Development of new therapeutic drugs offers promise for the treatment of many diseases, but effective and efficient delivery of drugs remains a significant challenge. Large molecule and protein-based drugs and vaccinations typically are administered via hypodermic needle since they cannot be absorbed through the skin or taken orally [1]. The requirement for trained health professionals, fear of needles, and the negative physiological impact of large and infrequent doses has motivated the development of alternative methods for delivering liquids through the skin that maintain therapeutic dosing simply and painlessly. Recent developments in the field of transdermal drug delivery [2] include iontophoresis [3], sonophoresis, microneedles [4], and chemical permeation enhancers [5], as well as renewed interest in

jet injectors [1,6–9]. Jet injectors, which propel liquids at speeds sufficient to penetrate skin without needles, were initially developed in the 1940s. Despite the great need for needle-free injection methods, jet injectors have remained largely underused due to concerns over potential cross contamination due to splash-back [10], unreliability of dose and depth of delivery [11,12], and painful bruising and bleeding [13,14]. It has been argued that the lack of reliability arises primarily from the inability of current devices to respond to variations in skin mechanical properties [11] and is exacerbated by the large dose sizes (tens to hundreds of microliters) and nozzle diameters (100–500 μm) employed by conventional injectors [13], which also likely contribute to the problems of splash-back and pain.

A jet injector device that is capable of delivering electronically-controlled doses may offer improved consistency and reduced pain. We present and characterize a new needle-free microjet injector powered by the rapid expansion of a piezoelectric actuator that offers electronic control of fluid displacement. Neither conventional jet injectors powered by springs and compressed air, nor our

* Corresponding author. 608 Stanley Hall, Berkeley CA, 94720-3220, United States. Tel.: +1 510 643 5624; fax: +1 510 642 5587.

E-mail address: fletch@berkeley.edu (D.A. Fletcher).

previous bubble-driven device [15,16], have offered electronic control of the injection speed. A recent report has demonstrated that fluid jets generated by piezoelectric actuators are capable of skin penetration and delivery of insulin into animals [17]. However, this work did not demonstrate electronic variation of the actuator expansion rate, a key enabling feature of our device. Further, the physical mechanisms of fluid pressurization, jet formation, and material penetration by an electronically-controlled jet injector are at present unclear. A precise understanding of these mechanisms is a critical next step toward the effective clinical application of piezoelectric powered needle-free transdermal drug delivery devices and is the focus of this paper.

Our new device offers electronic control of the actuator expansion rate over nearly an order of magnitude to achieve higher speeds and larger doses than previously reported, and the device is instrumented for the detection of jet velocity (strobe microscopy), actuator and plunger motion (laser-based motion tracking), and jet impact force (miniature load cell). We utilize experimental and computational methods to evaluate the efficacy of our device and the degree to which electronic control of the actuator expansion rate facilitates control of the injection characteristics (expelled volume, pressure, penetration depth). We show that our piezoelectric microjet is capable of propelling fluid jets of small diameter (40–130 μm) and volume (50–650 nL) to high speeds (60–160 m/s) and high impact pressures (0.3–3 MPa) capable of penetrating materials that model the elastic properties of the skin. We conclude with a discussion of the potential for achieving more reliable jet injection through the use of electronically-controlled actuators.

2. Materials and methods

2.1. Device

Our piezoelectric-driven needle-free injector, which we refer to as the piezoelectric microjet, consisted of a conventional syringe fitted with a micro-nozzle and completely filled with liquid. The syringe plunger was placed in mechanical contact with a conventional piezoelectric multi-layer actuator (Fig. 1A). Glass syringes with an inner diameter of 1.457 mm and 100 μL capacity were used (Hamilton, Reno, NV). Micro-nozzles were fabricated using a micropipette puller (Sutter Instruments, Novato, CA) to thermally draw 1.50 mm outer diameter, 0.86 mm inner diameter borosilicate glass capillary tubing. The tip of the drawn capillary was subsequently melted shut, reopened to the desired nozzle diameter by sanding, cut to a length of about 2.5 mm, and adhered over the tip of a detachable syringe needle (cut to about 4 mm in length) using epoxy resin (Devcon Epoxy, Danvers, MA). Nozzle diameters made by this method were varied from 30 μm to 132 μm . The inner diameter of the syringe needle was 260 μm (Hamilton, Reno, NV). The syringe plunger and barrel rely on a very close mechanical fit (as opposed to a deformable plunger tip material found in conventional syringes) to limit liquid loss around the plunger. Liquids ejected from the microjet included deionized water and ethanol (Rossville Gold Shield, Hayward, CA). All liquids were degassed and filtered. Just prior to each use, examination under low power light microscopy (20 X) was used

to ensure that no air bubbles were present inside the device. The volume within the syringe during microjet actuation was controlled from 4 μL to 20 μL within approximately 0.5 μL . A lead zirconium titanate (PZT) piezoelectric actuator, rated for $17.4 \pm 2 \mu\text{m}$ expansion at 150 V (Thorlabs, Newton, NJ), was used to actuate the microjet device. During microjet operation, a voltage pulse from a custom power supply caused rapid expansion of the actuator. The power supply was electrically equivalent to a resistor (R) and capacitor (C_p) (piezoelectric capacitance, 1.4 μF) in series with an ideal voltage source (Fig. 1A). The voltage rise after actuation closely followed the equation for a charging capacitor, $V(t) = V_s (1 - \exp(-t/\tau))$, with time constants $\tau = R * C_p$ varying from 0.96 μs to 27 μs as R was varied from ~ 0 to 20 Ω . The observed time constants exceeded expected constants by an average value of 1.4 μs , likely due to a combination of parasitic resistance and capacitance in the charging circuit.

2.2. Strobe microscopy

Initial jet velocities were measured using a strobe microscopy technique in which two LED flashes of 0.5 μs duration spaced 5 μs apart captured two images of the jet leading edge on a single exposure of a cooled CCD camera (Qimaging, Burnaby, BC) (Fig. 1A,B) [8,10]. By measuring the distance between the two images and dividing by their time separation, the average velocity

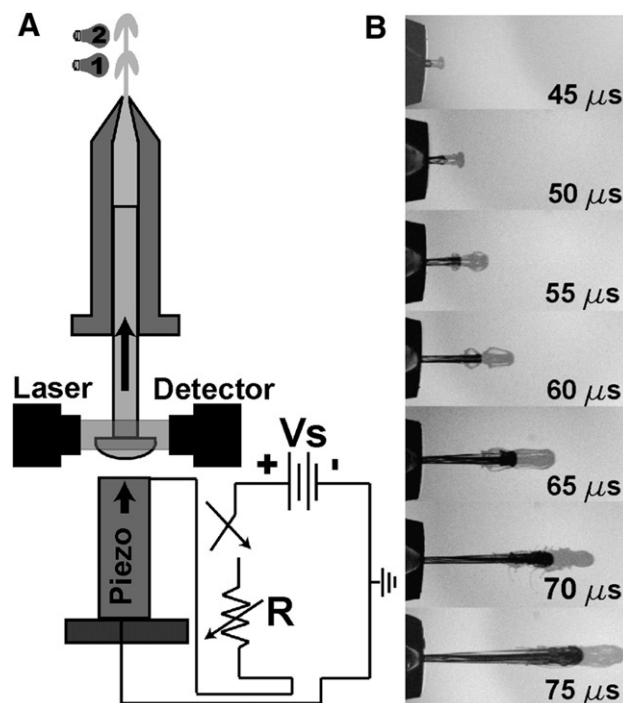


Fig. 1. The piezoelectric microjet. (A) Schematic diagram of the piezoelectric microjet. A resistive–capacitive circuit controls the expansion of the piezoelectric actuator. A laser-based tracking mechanism is used to record the motion of the syringe plunger. A two-flash strobe microscopy technique is used to capture the development of the jet. (B) Images of the jet emerging from the microfluidic nozzle captured using strobe microscopy. The time listed on each photograph is the time of the first strobe pulse. The second strobe pulse occurred 5 μs after the time shown.

of the jet leading edge during the elapsed time was derived. This technique was useful during the first 100–120 μs after piezo actuation. After longer times, the jet traveled outside the camera's field of view, making the determination of jet velocity difficult. For the measurement of jet velocity as a function of initial plunger velocity (Fig. 5C), water was used as the working fluid (density: 997 kg/m^3 [18], bulk modulus: 2.18 Gpa [19]). For the measurement of jet velocity as a function of nozzle diameter and initial chamber volume (Fig. 5A, B), ethanol was used as the working fluid (density 785 kg/m^3 [18], bulk modulus: 894 Mpa [20]). Ethanol was used in these studies because its relatively low surface tension helped reduce problems with the trapping of air bubbles in the microjet nozzles, which was a particular concern for the smallest nozzles (40 μm) used.

2.3. Laser-based motion tracking

Laser-based motion tracking was used to examine the expansion of the piezoelectric actuator and the resulting motion of the syringe plunger (Fig. 1). A diode laser was directed across an edge of the moving object of interest and into a photodetector (Thorlabs, Newton, NJ) such that the moving object partially obscured the detector. In this way, motion of the object resulted in a change in voltage read at the detector. A micrometer stage (Thorlabs, Newton, NJ) was used to displace the object by known distances, creating a calibration between detector voltage and object position. Motion tracking of the plunger was carried out using the linear portion of this calibration.

2.4. Impact force measurements

To track the force and pressure exerted by the fluid jet over the course of an injection, we impinged the jet on a miniature load cell (10 kHz, 500 mN capacity, Honeywell Sensotec, Columbus, OH) (Fig. 2A). The separation between the microjet nozzle and the sensor surface was held constant at 1 mm. Estimates of the impact pressure were derived from impact force measurements by dividing the force by the nozzle area. Fig. 2B shows the variation of jet impact force with time for various nozzle diameters. Maximum impact force and average impact force were calculated from data such as these. Average force was determined by integrating the force vs. time trace above a threshold set at 10% of the maximum force and dividing by the time duration of the integration.

2.5. Expelled volume measurements

The total volume expelled during an injection was measured after an injection using light microscopy and a DC-servo driven stage (Thorlabs, Newton, NJ) attached to the piezoelectric actuator. Immediately after the injection, the syringe was observed to contain no air, but a separation was created between the actuator and plunger arising from the forward travel of the plunger due to momentum gained from the actuator. The stage was moved at a low (5 $\mu\text{m/s}$), constant velocity while observing the nozzle. As soon as the actuator contacted the plunger, the air–liquid interface at the front of the nozzle was observed to

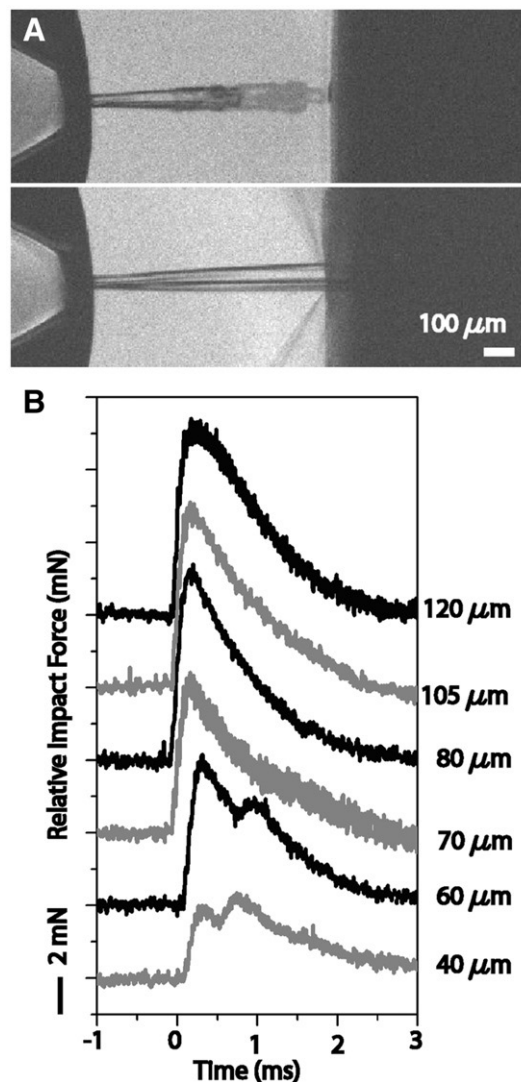


Fig. 2. (A) Fluid jet approaching (top) and impacting (bottom) the surface of a piezo-resistive load cell. (B) Typical load vs. time traces recorded by the load cell for various nozzle diameters. Chamber volume (6 μL) and charging characteristics (0 Ω , 150 V) were kept constant. Traces are vertically offset from each other for clarity.

move, and the stage was stopped. The total travel distance of the stage and the known syringe internal diameter were used to calculate the expelled volume within a standard deviation of approximately 10 nL.

2.6. Penetration depth measurements

Polyacrylamide gels were prepared by adding 10% ammonium persulfate and N,N,N',N' -tetramethylethylenediamine to 40% (w/v) acrylamide solution (Bio-Rad Laboratories, Hercules, CA) diluted with the appropriate amount of deionized water such that the final acrylamide concentration in the gel was controlled between 4 and 30 w/v%. The acrylamide solution consisted of acrylamide and bis-acrylamide in a ratio of 29:1 (Figs. 6C, 7B) or 37.5:1 (Fig. 7C) by mass. During the experiments, the gel was mounted in front of the microjet device with a standoff distance of 1 mm between the nozzle tip and gel. The piezoelectric microjet was fired directly

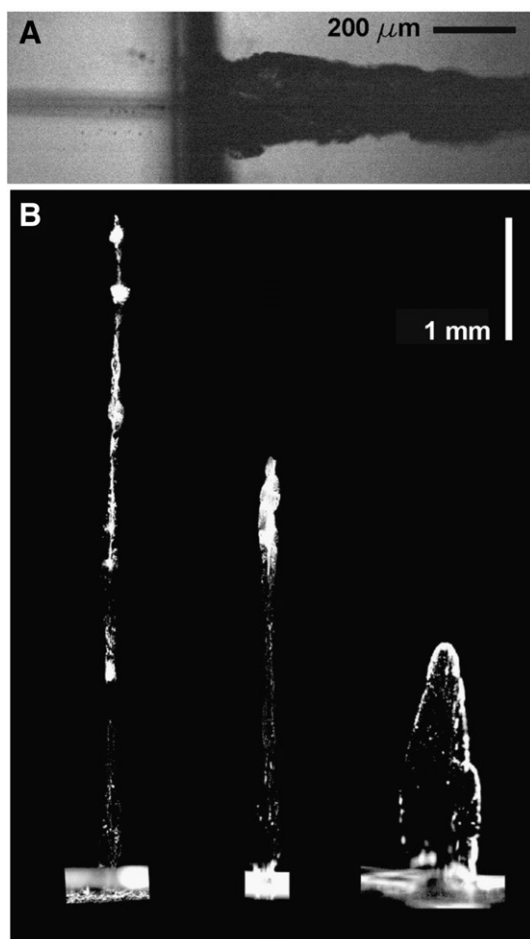


Fig. 3. (A) Fluid jet penetrating a gel sample. (B) Fluorescence micrographs of jet penetrations (150 V, 0 Ω , 6 μ L chamber volume) into 4 w/v% polyacrylamide gel using various nozzle diameters: 80 μ m (Left), 50 μ m (Center), 130 μ m (Right).

toward the gel surface (Fig. 3A). To visualize the penetration of the jet into the gel, fluorescent beads (500 nm FITC-conjugated latex beads, 2.69% solids by volume, Polysciences Inc., Warrington, PA) were diluted 100 \times in the injected fluid (water). Following the injections, fluorescent imaging of the gel (470 nm excitation, 535 nm emission) revealed the depth and morphology of the jet penetration (Fig. 3B).

3. Results and discussion

Our piezoelectric microjet uses the rapid expansion of a piezoelectric actuator to displace the plunger of a conventional syringe, generating a high-speed liquid jet of small diameter (30–130 μ m) capable of penetrating soft materials. We evaluated electronic control of this drug delivery device by (i) demonstrating control of jet velocity with the piezoelectric actuator; (ii) examining and modeling the effect of device parameter variation on the jet velocity; (iii) characterizing the dependence of the injection process on jet velocity and nozzle diameter; and (iv) demonstrating the device for penetration of skin model materials. Finally, we discuss strategies for the electronic control of drug delivery using piezoelectric jet injectors.

3.1. Control of jet velocity with the piezoelectric actuator

A fluid jet is created by the expansion of a conventional piezoelectric actuator against a syringe plunger, where the actuator and plunger are in contact but not physically coupled. In this way, the actuator and plunger travel together until the actuator expansion begins to slow down as it reaches its full travel (10–20 μ m depending on the applied charging voltage). At this point, the actuator oscillates about a mean position, while the plunger continues forward under momentum received from the actuator. Here we assume that the maximum (initial) plunger velocity is the velocity at which the plunger was traveling at the time of separation from the actuator. Variation of the initial plunger velocity represents the primary means of controlling the resulting injection process. Once the plunger separates from the actuator, the physical behavior of the device, which depends on geometrical and fluid properties, will determine the characteristics of the resulting injection. By controlling the initial plunger velocity we control the initial conditions of the injection. In contrast, by varying the device geometry, we adjust its physical response to these initial conditions.

The expansion of the piezoelectric actuator is controlled through variation of the charging circuit parameters. By varying charging circuit resistance (0–15 Ω) or charging voltage (80 V, 110 V, 150 V), we vary the voltage rise time and consequently the initial plunger velocity (0.2 m/s to 1 m/s), as illustrated in Fig. 4A,B. Here, charging voltage controls the extent of actuator expansion, and resistance controls the time constant over which the voltage rises, such that increases in charging voltage and/or decreases in resistance increase the initial plunger velocity. Initial plunger velocity varied approximately inversely with resistance (for fixed charging voltage, $R^2 \sim 0.93$) and proportionally with charging voltage (for fixed resistance, $R^2 \sim 0.95$) such that the relationship $v_{\text{plunger}} \propto dV/dt \propto V_0/R$ was obeyed. This relationship, where actuator displacement and voltage are proportional, is expected when the actuator stall force (850 N) greatly exceeds the maximum expected pressure force (<40 N based on jet speed) as is the case here. Fig. 4C shows the temporal evolution of jet velocity as a function of charging resistance, as measured using strobe microscopy. The maximum measured jet velocity increases significantly (50 m/s–140 m/s) with decreasing charging resistance, illustrating that electronic control of actuator expansion (0–15 Ω), and therefore initial plunger velocity, significantly impact the resulting fluid jet.

3.2. Effect of plunger velocity, nozzle diameter, and chamber volume on jet velocity

To better understand the process through which a syringe plunger traveling under an initial impulse of momentum creates a high-speed fluid jet, we compared jet velocities measured as a function of several device parameters with the predictions of a simplified fluid-dynamic model. Based on a model proposed by Baker et al. [7], we treat the microjet device as a fluid cylinder compressed by a moving mass with fluid exiting through a small orifice. This model considers the compressibility of the fluid, the inertia of the plunger, and mass loss through the orifice. Spatial pressure variation within the cylinder and

frictional losses in the device are neglected. A mass balance on the fluid leads to Eq. (1), where p represents pressure, B the bulk modulus of the fluid, x_p the relative motion of the plunger, ρ_o the fluid density at atmospheric pressure, A_o the orifice area, A_p the plunger area, and L the initial length of the fluid chamber. Here the first term on the right accounts for pressurization due to plunger motion, while the second term accounts for depressurization due to mass loss. Eq. (2) is a force balance on the plunger.

$$\frac{dp(t)}{dt} = \frac{(B + p(t)) \frac{dx_p(t)}{dt}}{L - x_p(t)} - \frac{BA_o}{A_p} \sqrt{\frac{2p(t)}{\rho_o}} \quad (1)$$

$$\frac{d^2x_p}{dt^2} = -\frac{A_p p(t)}{m_p} \quad (2)$$

The initial plunger velocity was taken from experiment (Fig. 4B). The initial pressure was estimated by solving Eq. (1) assuming a constant rate of actuator expansion from the resting to fully expanded condition. The expansion rate was assumed equal to the maximum plunger velocity (Fig. 4B). The system of equations and boundary conditions was solved using a Runge–Kutta method in Matlab, where the initial time was taken as the time at which the plunger separates from the actuator. Computational solution of the equation system resulted in prediction of the jet pressure and plunger position as functions of time. Predictions of jet velocity were derived from these jet pressures using the expression, $u_{jet}(t) = \sqrt{2p(t)/\rho_o}$, where u_{jet} represents the jet velocity. This expression derives from Bernoulli’s equation and consequently implies the neglect of frictional loss, compressibility, and unsteady acceleration along streamlines inside the nozzle.

Fig. 5 presents experimental and computational results for the variation of peak jet velocity with three parameters: initial plunger velocity, initial chamber volume, and nozzle diameter. In all cases the experimental data represent the peak jet velocity measured by strobe microscopy, while the computational data represent the peak predicted jet velocity. The figure insets display predictions of the variations in temporal evolution of jet velocity as functions of the same parameters. Examining Fig. 5A, computation predicts and experiments confirm that jet velocity increases monotonically as a function of increasing initial plunger velocity, where nozzle diameter was constant at 70 μm and the chamber volume was 6 μL .

Computational predictions indicate that increasing the initial chamber volume increases the system response time (time to peak jet velocity) and decreases the peak jet velocity (Fig. 5B), where nozzle diameter was constant at 40 μm and initial plunger velocity was maximized (0 Ω , 150 V). These effects arise directly from the compressibility of the fluid. The relatively low Mach numbers (jet velocity/speed of sound in water) associated with these fluid jets (0.02–0.03) do not immediately suggest the importance of compressibility. However, when one considers that the expected volumetric compression at the maximum observed pressures ($\sim 0.6\%$ of initial chamber volume) is approximately equivalent to the volume swept out by the plunger during actuator expansion ($\sim 0.5\%$ of initial chamber

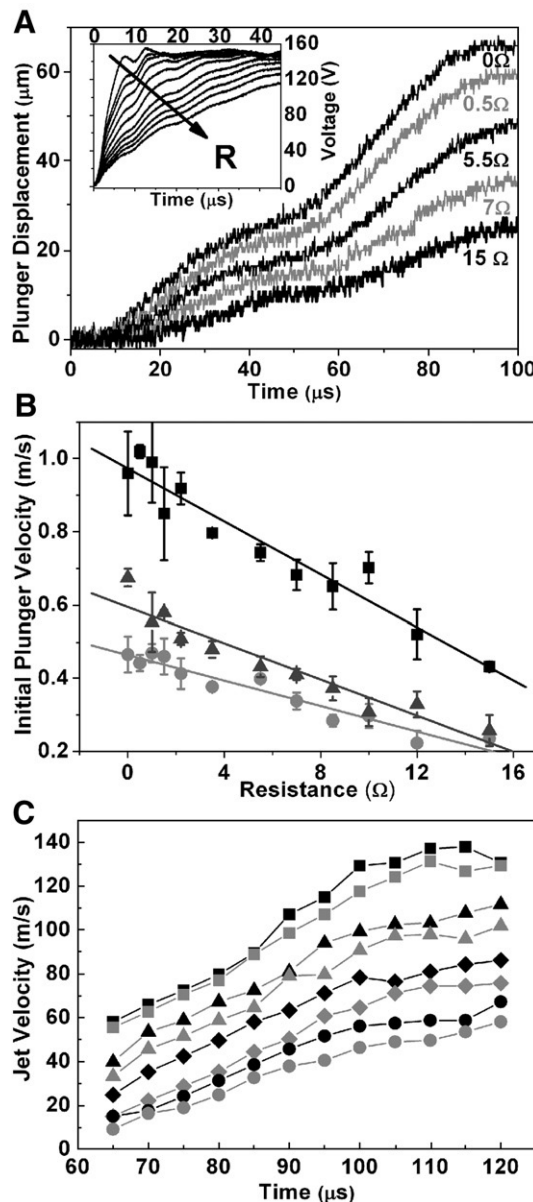


Fig. 4. (A) Initial plunger motion captured by laser-based tracking during piezoelectric actuation. (A-inset) Voltage rise across the piezoelectric actuator as a function of time for resistance increasing from 0 to 15 Ω (0, 0.5, 5.5, 7, 15 Ω). (B) Initial plunger velocity as a function of resistance for three charging voltages: 80 V (\blacksquare), 110 V (\blacktriangle), 150 V (\bullet). Error bars are plus and minus one standard deviation, where $N=3$ to 6 per point. (C) Jet velocity captured by strobe microscopy as a function of the time after piezo actuation for charging resistances: 0 (\blacksquare), 1 (\blacksquare), 3 (\blacktriangle), 5 (\blacktriangle), 8 (\blacklozenge), 12 (\blacklozenge), 15 (\bullet), 20 Ω (\bullet) and 150 V charging voltage. The nozzle diameter and initial chamber volume were 70 μm and 6 μL , respectively.

volume), the importance of compressibility is clear. The experimentally observed decrease in peak velocity with increasing chamber volume confirms the importance of including fluid compressibility in this analysis (Fig. 5B).

Finally, peak jet velocity decreased with increasing nozzle diameter (Fig. 5C) for a chamber volume of 6 μL and maximum initial plunger velocity (0 Ω , 150 V). Increasing nozzle diameter led to greater mass loss and thus lower peak jet velocity and greater

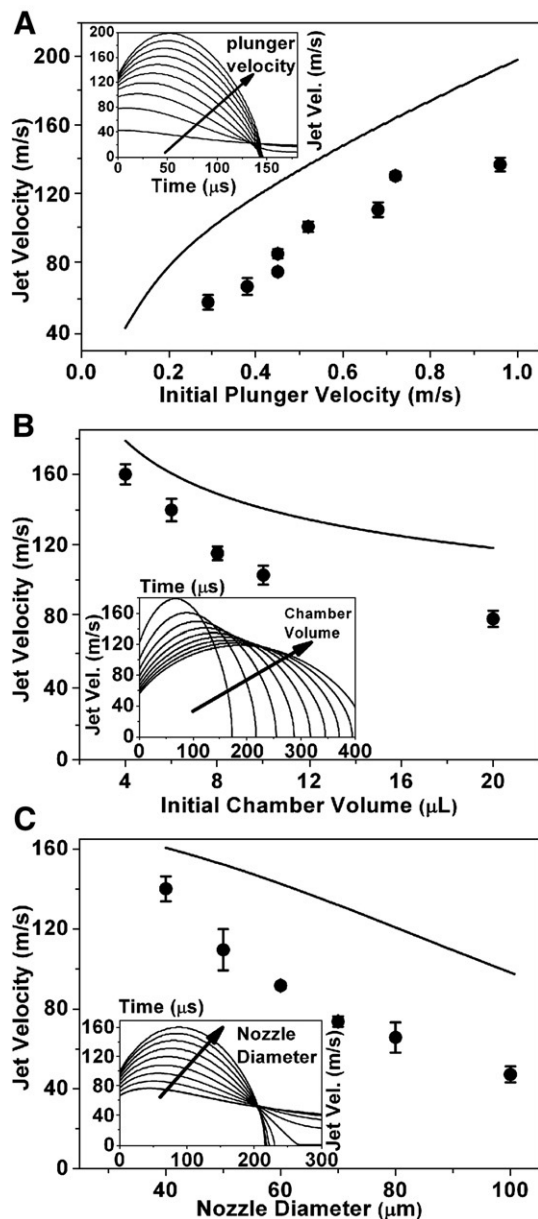


Fig. 5. Maximum measured jet velocity and maximum predicted jet velocity as a function of device parameters including initial plunger velocity (A), initial chamber volume (B), and nozzle diameter (C). (Insets) Predicted jet velocity as a function of time for parameter variations including nozzle diameter (A-inset), initial chamber volume (B-inset), and initial plunger velocity (C-inset). For all graphs error bars represent plus and minus one standard deviation, where $N=3$ to 5 per point.

damping. Computational results predict a transition from under-damped (oscillatory) to over-damped (non-oscillatory) behavior of the system as nozzle diameter increases (Fig. 5C-inset). The existence of this transition was confirmed by the load cell data presented in Fig. 2B, and it appeared to occur between nozzle diameters of 60 μm and 70 μm.

On average, the model predicts peak jet velocities that are within approximately 50% of measured velocities. This difference likely arises from two sources. First, the shapes of the impact force traces (Fig. 2B) that follow the entire injection, suggest that the jet velocity likely continues to increase at times

later (300–500 μs) than those examined by strobe microscopy (~120 μs). In this way, the experimental data in Fig. 5 is likely consistently lower than the true peak jet velocity. Second, frictional losses, which decrease jet velocity, are not included in the model. Neglect of frictional losses is partially justified by evaluating the non-dimensional number, vt/r_0^2 , which compares the diffusion of vorticity (boundary layer growth) with the device dimensions. When this parameter has a value significantly less than one, boundary layers are small relative to the device dimensions, implying that frictional losses are small compared to the magnitudes they would attain for developed flow [21]. When the nozzle radius is taken as the length scale and the time is chosen as 100 μs (time course of strobe measurements), the value of vt/r_0^2 is much less than one (0.02–0.2). Despite these sources of error, the model and data agree qualitatively, suggesting that the microjet device behaves much as the model describes.

3.3. Variation of injection characteristics with plunger velocity and nozzle diameter

The reliability of jet-based injections depends upon the control of the depth and dose of drug delivery. Having demonstrated electronic control of the jet velocity, we now seek to evaluate the extent to which this capability is useful for controlling the resulting injection. To this end, we measure three relevant injection characteristics (expelled volume, impact pressure, and penetration depth in a soft model material) as functions of initial plunger velocity (our control parameter) and nozzle diameter (an important geometrical parameter). Measurements of total expelled volume correspond to the maximum possible drug dose. Impact pressure measurements are useful estimates of the stress applied by the jet to the surface of a material. In order for penetration to occur, impact pressure must exceed the critical stress for material failure. By correlating measurements of expelled volume and impact pressure with measurements of penetration depth in a soft model material (4 w/v% polyacrylamide gel), we gain insight into the penetration process. We expect penetration depth to depend upon energy delivery to the material, when impact pressure exceeds the critical stress. The total energy delivery during the injection is roughly the time integral of the product of jet pressure and volumetric flow rate, which we expect to vary strongly with jet velocity and nozzle diameter. Thus, the total penetration depth in a model material will likely vary significantly with initial plunger velocity and nozzle diameter. We quantify this variation and interpret it based on the variation in impact pressure and expelled volume.

Fig. 6 examines the impact of varying initial plunger velocity (0.2–1 m/s) on the injection characteristics. Variation of plunger speed was accomplished by varying circuit resistance at three different charging voltages (80, 110, 150 V). Impact force measurements taken at each of these three voltages fall approximately along a single curve relating impact force and initial plunger speed (Fig. 6A). Total expelled volume initially increases and then comes roughly to a plateau as initial plunger velocity increases (Fig. 6B). Data resulting from different charging voltages fall along a single trend relating expelled

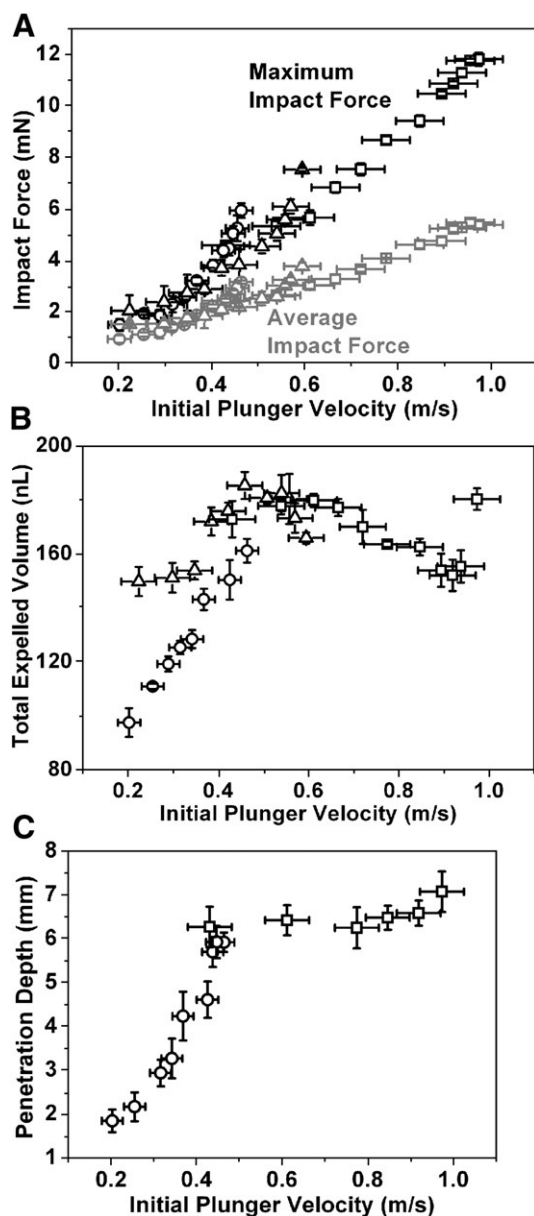


Fig. 6. Injection characteristics as a function of initial plunger velocity (0.2 m/s–1 m/s). Nozzle diameter was approximately 82 μm , and chamber volume was 6 μL for all studies. Jet velocities were varied by varying charging voltage (80 V (\circ , \odot), 110 V (\triangle , \triangleleft), 150 V (\square , \square)) and resistance (0–15 Ω). (A) Maximum and average impact pressure as a function of initial plunger velocity. Error bars represent plus and minus one standard deviation, where $N=3$ to 5 per point. (B) Total expelled volume as a function of initial plunger velocity. Error bars represent plus and minus one standard deviation, where $N=7$ to 12 per point. (C) Penetration depth in 4 w/v% PAG as a function of initial plunger velocity. Error bars represent plus and minus one standard deviation, where $N=8$ to 11 per point.

volume to initial plunger velocity. The existence of single trends relating impact force and expelled volume to initial plunger velocity suggests that various combinations of voltage and resistance, which result in the same initial plunger velocity, will result in injections with very similar characteristics. The lack of significant increase in expelled volume beyond an initial plunger velocity of about 0.5 m/s is likely due to the increasing importance of frictional losses and loss of fluid around the

syringe plunger as the device internal pressure increases. Penetration depth in soft matter initially increases strongly with increasing initial plunger velocity and then increases more slowly, with the rate transition occurring at an initial plunger velocity of approximately 0.5 m/s (Fig. 6C). As discussed above, penetration depth ought to increase with increasing energy delivery (product of pressure and volumetric flow rate) above the critical stress for material failure. In this way, we expect the penetration depth to increase monotonically with increasing initial plunger velocity. Further, we expect the rate of increase to decrease once expelled volume reaches a plateau. These results illustrate that increase of initial plunger velocity from 0.2 to 1 m/s results in significant increases in impact force (1–12 mN), expelled volume (90–180 nL) and penetration depth (1–8 mm), none of which is independent.

Fig. 7 reveals the impact of varying nozzle diameter (30–132 μm) on the injection characteristics. In all experiments the charging voltage was approximately 150 V and no additional series resistance was applied (0 Ω) such that the initial plunger velocity was approximately 1 m/s. Initial plunger velocity was observed to remain constant with variations in nozzle diameter (data not shown). Nozzle diameter is an important device parameter because it greatly impacts the maximum jet velocity (Fig. 5A) and greatly influences the area over which the jet acts on a material. Average and maximum impact pressure decrease strongly (3.2–0.4 MPa) with increasing nozzle diameter, while expelled volume increases strongly (50–650 nL) with increasing nozzle diameter (Fig. 7A). The large (1300%) increase in expelled volume with increasing nozzle diameter suggests that frictional effects, greatly accentuated at small nozzle diameters, are important in stopping the plunger and thus limiting the expelled volume. Additionally, as the nozzle diameter increases, jet velocity decreases and thus the pressure pushing back on the traveling plunger decreases, increasing plunger travel. Penetration depth varies with nozzle diameter according to a complex trend. Depth increases from 30 to 45 μm , decreases between 45 and 50 μm , increases from 50 to 80 μm and then decreases for increasing nozzle diameter greater than 80 μm . Maximum penetration depth is achieved roughly equally using 40, 45, and 80 μm nozzles. To confirm that the trend in penetration depth did not arise from irregularities in the nozzle, two nozzles each of diameter 40, 50, and 80 μm were tested. In all cases, the trend reported here (Fig. 7B) was observed (data not shown). The decrease in penetration depth for nozzle diameters greater than 80 μm likely occurs because, while the volume delivery using these diameters is large, the rapidly falling pressure with increasing diameter indicates that much of this volume is likely delivered at pressures below the critical stress for material failure. The increase in penetration depth from 30 μm to 40 μm may occur due to increasing volume delivery and decreasing frictional losses that occur as nozzle diameter increases. The variation in penetration depth from 40 μm to 80 μm is likely the result of multiple complex and coupled processes including the transient nature of the jet velocity, the pressure dependence of the material erosion rate, the transition from under-damped to over-damped system behavior, and the likely strong dependence of viscous losses on nozzle diameter. Clearly impact pressure, expelled volume, and penetration depth vary strongly and dependently with nozzle diameter.

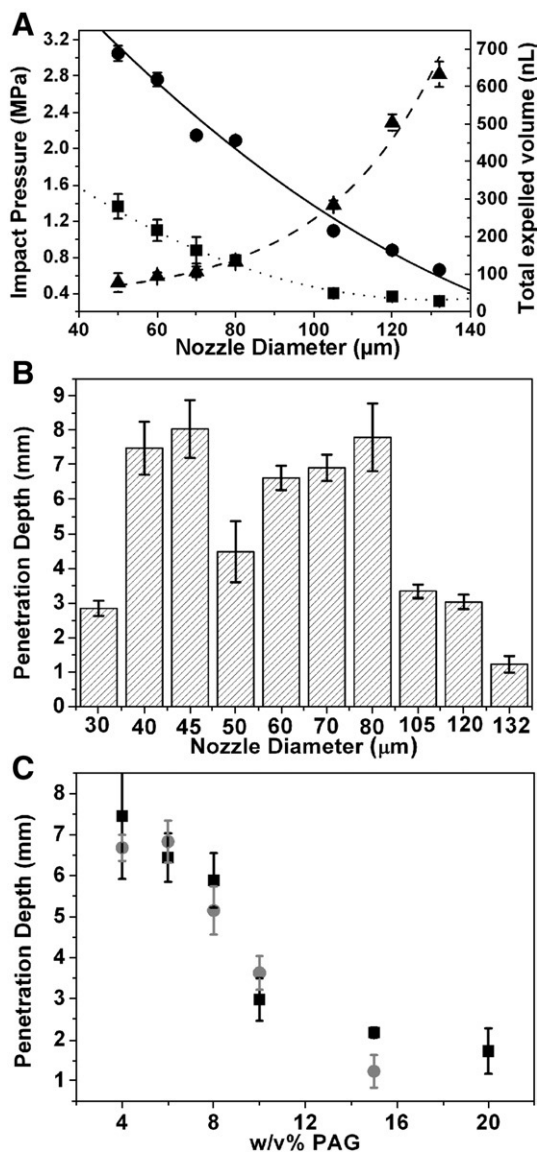


Fig. 7. (A) Injection characteristics as a function of nozzle diameter (30 μm –132 μm). Initial plunger velocity was approximately 1 m/s (150 V, 0 Ω), and chamber volume was 6 μL for all studies. Maximum (●) and average (■) impact pressure and total expelled volume (▲) as a function of nozzle diameter. Non-linear trend lines are added in order to guide the eye. Error bars represent plus and minus one standard deviation for all graphs. For impact pressure data, $N=3$ to 5 per point. For expelled volume, $N=7$ to 12. (B) Penetration depth in 4 w/v% PAG as a function of nozzle diameter. The number of samples was 8 to 11 per point. (C) Penetration depth as a function of gel acrylamide content (4, 6, 8, 10, 15, 20 w/v%) using 40 μm (■) and 80 μm (●) diameter nozzles. Initial plunger velocity was approximately 1 m/s (150 V, 0 Ω), and chamber volume was 6 μL for all studies. The number of samples was 8 to 11 per point.

3.4. Penetration of soft tissue model materials

To evaluate the capacity of the piezoelectric microjet to deliver drugs through the skin and underlying soft tissue, we tested the penetration depth in an array of soft materials, which vary in elastic modulus and strength over a range that coincides with the reported values of these material properties for skin. The skin is a complex, inhomogeneous material [22].

Measurements of its mechanical properties vary considerably with age of the patient and anatomical site of the sample as well as the testing procedure [23–29]. The elastic modulus of whole skin has been reported to range from 20 kPa to tens of megapascals [27]. The critical stress of the dermis has been reported to range from 500 kPa to 2 MPa [24]. Notably, the impact pressures achieved by our device exceed this range when nozzles of diameter less than 80 μm are used (Fig. 7A). Polyacrylamide gels having acrylamide content ranging from 4% to 30% served as model materials. The elastic moduli of these materials have been reported in the range of 10 to 500 kPa, where modulus increases with increasing acrylamide content [8,30]. The critical stress of these materials has been reported to range from 30 kPa to greater than 1.5 MPa, where critical stress increases with increasing acrylamide content [31]. We note that the most superficial layer of the skin, the stratum corneum, which is thin (~ 10 – 15 μm) and consists of dense anucleate cells, is known to have a higher fracture stress than other layers of the skin and thus may impose an additional energy barrier to skin penetration not accounted for in our gel models. The penetration depth achieved by the piezoelectric microjet into the model materials was measured at maximum initial plunger velocity (150 V, 0 Ω) using the 40 and 80 μm diameter nozzles (Fig. 7C). These nozzles were chosen because they achieved the maximum penetration depth during the injection characterization study (Fig. 7B). For both nozzles, penetration depth decreases continuously with increasing acrylamide content of the gel. The 80 μm nozzle was capable of penetrating 15% gels but could not penetrate 20% gels. The 40 μm nozzle was capable of penetrating 20% gels but could not penetrate 30% gels. Interestingly, the depth of penetration achieved by the 40 μm and 80 μm nozzles remains approximately the same over a wide range of material stiffness. The typical widths of penetrations into gel increased with increasing acrylamide content of the gel (80 μm average for 4 w/v% gel to 220 μm for 20 w/v% gel), data not shown. The aspect ratio (penetration depth / typical penetration width) decreased significantly (80 on average for 4 w/v% gel to 10 on average for 20 w/v% gel) with acrylamide content of the gel, data not shown. These trends likely arise due to the increased residence time of the jet per unit length of penetrations as the gel stiffness and strength increased (penetration depth decreased). We note that, while gel materials provide a useful model for the process of material penetration in skin, they do not match the diffusivity and porosity of skin and thus do not model the process of drug dispersion in the skin. Conventional jet injectors have been characterized extensively according to their penetration depth in 10%–30% polyacrylamide gels [8,9]. In these studies, penetration depth increased from about 1 to 13 mm as acrylamide content decreased from 30 to 10 w/v% [8]. While the jet velocities achieved using our device are comparable to those produced by conventional injectors (~ 170 m/s) [8], the penetration depths we achieve are somewhat less than those reported for conventional injectors. This reduced penetration depth likely arises because our nozzle diameters (40,80 μm vs. 152 μm) and shot durations (~ 1 ms vs. greater than 20 ms) are significantly less than those used with

conventional injectors such that the total energy of the injection is much less. In this way, our results suggest that significant reductions in injection energy may be possible while maintaining the potential for skin penetration.

3.5. Strategies for controlled drug delivery using electronic jet injectors

Conventional needle-free jet injectors, which produce jets of approximately constant velocity throughout each injection, have encountered difficulty in controlling the depth and dose of drug delivery [11,12]. Fluid jets from these devices deposit into the skin in three stages: (i) a penetration stage in which the injection depth is defined followed by (ii) a stagnation event and (iii) a constant depth dispersion stage during which fluid (drug) is absorbed by the penetrated tissue surfaces [6,8,9]. If the jet speed is too low, penetration of dense superficial layers does not occur, and no drug dose is received. If it is too high, the skin is not able to absorb all the fluid entering it. In this case, much fluid overflow occurs resulting in an unreliable dose. Variability in skin properties between individuals and between various parts of the body makes control of depth and dose using a single jet velocity very difficult. In contrast to conventional jet injection devices, which typically deliver tens to hundreds of microliters in a single injection [1], we have demonstrated that the piezoelectric microjet device delivers much smaller doses ranging from 50 nL to 650 nL, the velocity of which is controlled electronically. In this way, effective use of the microjet device is likely to rely upon the delivery of multiple doses. When multiple injections are used, the ability to continuously vary the jet velocity from shot to shot by varying the charging voltage and resistance could be used to create a time-varying velocity profile of the injection. Here, the initial injections might occur at a relatively high velocity chosen to achieve a desired stagnation depth. Once the stagnation depth is reached, subsequent injections might occur at a relatively low velocity in order to deliver the desired dose without the risk of overflow. As a result, a device that is capable of precisely controlling the jet pressure over time may improve the reliability of jet-based injections. Further, by delivering multiple doses, it is possible to fully decouple injection velocity from total injection volume, which should enable independent control of the depth and dose of drug delivery [17]. Our ongoing work involves both the use of the device described here to deliver multiple injections and the development of a device capable of larger volume injections for which the velocity varies during each injection.

4. Conclusions

We have presented a piezoelectric microjet injector with electronic control over actuator expansion, which is capable of penetrating soft tissue model materials. The behavior of the injector system agrees qualitatively with the predictions of a simple fluid-dynamic model, which considers fluid compressibility, plunger inertia, and mass loss. We have shown that by controlling actuator expansion, we are able to gain significant

dependent control over injection characteristics such as jet velocity, impact pressure, expelled volume, and depth of penetration in model materials, parameters which are inherently coupled. Finally, we argue that electronic control of jet injections creates the opportunity to vary the jet pressure over the course of an injection, which may significantly improve the reliability of jet-based injections and effectively decouple injection parameters such as the depth and dose of drug delivery.

Acknowledgements

The authors gratefully acknowledge Professor Samir Mitra-gotri and Giovanni Nisato for useful discussions as well as Philips Semiconductor (NXP) and StrataGent Life Sciences for generous financial support. J.C.S. gratefully acknowledges fellowship support from the NSF Graduate Research Fellowship Program and from the ARCS Foundation.

Disclosure: D.A.F is a stockholder in StrataGent.

References

- [1] S. Mitragotri, Immunization without needles, *Nat. Rev., Immunol.* 5 (12) (2005) 905–916.
- [2] M.R. Prausnitz, S. Mitragotri, R. Langer, Current status and future potential of transdermal drug delivery, *Nat. Rev. Drug Discov.* 3 (2) (2004) 115–124.
- [3] X.M. Wu, H. Todo, K. Sugibayashi, Enhancement of skin permeation of high molecular compounds by a combination of microneedle pretreatment and iontophoresis, *J. Control. Release* 118 (2) (2007) 189–195.
- [4] H.S. Gill, M.R. Prausnitz, Coated microneedles for transdermal delivery, *J. Control. Release* 117 (2) (2007) 227–237.
- [5] P. Karande, A. Jain, S. Mitragotri, Insights into synergistic interactions in binary mixtures of chemical permeation enhancers for transdermal drug delivery, *J. Control. Release* 115 (1) (2006) 85–93.
- [6] J. Baxter, S. Mitragotri, Jet-induced skin puncture and its impact on needle-free jet injections: experimental studies and a predictive model, *J. Control. Release* 106 (3) (2005) 361–373.
- [7] A.B. Baker, J.E. Sanders, Fluid mechanics analysis of a spring-loaded jet injector, *IEEE Trans. Biomed. Eng.* 46 (2) (1999) 235–242.
- [8] J. Schramm-Baxter, J. Katrencik, S. Mitragotri, Jet injection into polyacrylamide gels: investigation of jet injection mechanics, *J. Biomech.* 37 (8) (2004) 1181–1188.
- [9] J. Schramm-Baxter, S. Mitragotri, Needle-free jet injections: dependence of jet penetration and dispersion in the skin on jet power, *J. Control. Release* 97 (3) (2004) 527–535.
- [10] P.N. Hoffman, R.A. Abuknesha, N.J. Andrews, D. Samuel, J.S. Lloyd, A model to assess the infection potential of jet injectors used in mass immunisation, *Vaccine* 19 (28–29) (2001) 4020–4027.
- [11] J. Schramm, S. Mitragotri, Transdermal drug delivery by jet injectors: energetics of jet formation and penetration, *Pharm. Res.* 19 (11) (2002) 1673–1679.
- [12] G.E. Theintz, P.C. Sizonenko, Risks of jet injection of insulin in children, *Eur. J. Pediatr.* 150 (8) (1991) 554–556.
- [13] S. Mitragotri, Innovation—current status and future prospects of needle-free liquid jet injectors, *Nat. Rev. Drug Discov.* 5 (7) (2006) 543–548.
- [14] U. Schneider, R. Birnbacher, E. Schober, Painfulness of needle and jet injection in children with diabetes-mellitus, *Eur. J. Pediatr.* 153 (6) (1994) 409–410.
- [15] D.A. Fletcher, D.V. Palanker, Pulsed liquid microjet for microsurgery, *Appl. Phys. Lett.* 78 (13) (2001) 1933–1935.
- [16] D.A. Fletcher, et al., Intravascular drug delivery with a pulsed liquid microjet, *Arch. Ophthalmol-Chic.* 120 (9) (2002) 1206–1208.
- [17] A. Arora, et al., Needle-free delivery of macromolecules across the skin by nanoliter-volume pulsed microjets, *Proc. Natl. Acad. Sci. U. S. A.* 104 (11) (2007) 4255–4260.

- [18] R.E. Bolz, G.L. Tuve, CRC Handbook of Tables for Applied Engineering Science, CRC Press, Boca, Raton, FL, 1973.
- [19] W.P. Graebel, Engineering Fluid Mechanics, Taylor & Francis, New York, NY, 2001.
- [20] D.R. Lide, CRC Handbook of Chemistry and Physics, CRC Press, Boca Raton, FL, 2001.
- [21] F.M. White, Viscous Fluid Flow, McGraw-Hill, New York, NY, 2006.
- [22] L.A. Goldsmith, Physiology, Biochemistry, and Molecular Biology of the Skin, Oxford University Press, New York, NY, 1991.
- [23] Please check: M.E. Nimni, E. Deguia, L.A. Bavetta, Collagen hexosamine and tensile strength of rabbit skin during aging, *J. Invest. Dermatol.* 47 (2) (1966) 156–158.
- [24] H. Holzmann, G.W. Korting, D. Kobelt, H.G. Vogel, Studies on mechanical properties of human skin in relation to age and sex, *Arch. Klin. Exp. Dermatol.* 239 (4) (1971) 355–367.
- [25] H.G. Vogel, Correlation between tensile-strength and collagen content in rat skin—effect of age and cortisol treatment, *Connect Tissue Res.* 2 (3) (1974) 177–182.
- [26] H.G. Vogel, Tensile-strength, relaxation and mechanical recovery in rat skin as influenced by maturation and age, *J. Med.* 7 (2) (1976) 177–188.
- [27] S. Diridollou, et al., In vivo model of the mechanical properties of the human skin under suction, *Skin Res. Technol.* 6 (4) (2000) 214–221.
- [28] Y.S. Papir, K.H. Hsu, R.H. Wildnauer, Mechanical-properties of stratum-corneum. 1. Effect of water and ambient-temperature on tensile properties of newborn rat stratum-corneum, *Biochim. Biophys. Acta* 399 (1) (1975) 170–180.
- [29] K.S. Koutroupi, J.C. Barbenel, Mechanical and failure behavior of the stratum-corneum, *J. Biomech.* 23 (3) (1990) 281–287.
- [30] E.A. Brujan, K. Nahen, P. Schmidt, A. Vogel, Dynamics of laser-induced cavitation bubbles near elastic boundaries: influence of the elastic modulus, *J. Fluid Mech.* 433 (2001) 283–314.
- [31] G.G. Ferruzzi, N. Pan, W.H. Casey, Mechanical properties of gellan and polyacrylamide gels with implications for soil stabilization, *Soil Sci.* 165 (10) (2000) 778–792.